ADVANCED MATERIALS INTERFACES

www.advmatinterfaces.de

Femtosecond Laser Direct Writing of Porous Network Microstructures for Fabricating Super-Slippery Surfaces with Excellent Liquid Repellence and Anti-Cell Proliferation

Jiale Yong, Jinglan Huo, Qing Yang, Feng Chen, Yao Fang, Xingjuan Wu, Lin Liu, Xiaoyun Lu,* Jingzhou Zhang, and Xun Hou*

In this paper, it is demonstrated that one-step femtosecond laser ablation can be used to directly fabricate porous network microstructures on various polymer surfaces, including poly(ethylene terephthalate) (PET), poly(methyl methacrylate), polyamide, polycarbonate, polyethylene, and polylactic acid. Taking PET as an example, following femtosecond laser ablation, the PET surface is fully covered by large numbers of interconnected pores with a diameter of several hundred nanometers. The chemical treatment of the porous surface for further lowering of its surface free energy and infusion with lubricating liquid led to the successful fabrication of a slippery surface. The as-synthesized slippery surface showed excellent liquid-repellent ability; various liquids are demonstrated to freely slide down such a surface. Compared to previously reported slippery surfaces, the femtosecond laser-induced slippery surface consists of a porous layer and substrate layer that are inherently one material. Furthermore, it is found that the use of the original laser-induced porous PET surface as a culture substrate is able to promote the growth of C6 glioma cells, while the slippery PET surface completely inhibits C6 glioma cell growth. It is revealed that femtosecond laser direct writing can be used as a general method to form porous microstructures on various polymer surfaces.

Dr. J. Yong, Dr. J. Huo, Prof. F. Chen, Dr. Y. Fang, Dr. J. Zhang, Prof. X. Hou
State Key Laboratory for Manufacturing System Engineering and Key Laboratory of Photonics Technology for Information of Shaanxi Province
School of Electronics and Information Engineering
Xi'an Jiaotong University
Xi'an 710049, P. R. China
E-mail: chenfeng@mail.xjtu.edu.cn

Prof. Q. Yang
School of Mechanical Engineering
Xi'an Jiaotong University
Xi'an 710049, P. R. China

X. Wu, L. Liu, Prof. X. Lu
Key Laboratory of Biomedical Information Engineering of Ministry of Education
School of Life Science and Technology
Xi'an Jiaotong University
Xi'an 710049, P. R. China
E-mail: luxy05@mail.xjtu.edu.cn

The ORCID identification number(s) for the author(s) of this article can be found under https://doi.org/10.1002/admi.201701479.

DOI: 10.1002/admi.201701479

Porous materials have prospects for broad application in areas such as catalysis, adsorption, separation, ion exchange, biomedicine, energy, environment, and photoelectric materials, due to their high specific surface area, uniform and tunable pore size, and structural diversity.[1–3] The design and fabrication of porous microstructures with sizes down to the micro-/nanoscale have recently become one of the most active research areas. Among porous materials, porous polymers in particular have attracted a growing level of interest due to the potential for combining characteristics of both polymers and porous microstructures.[1,3] Typical methods developed for fabricating such types of porous microstructures include direct templating,[4,5] block copolymer self-assembly,[6,7] direct synthesis,[8] high internal phase emulsion polymerization,[9] breath figures,[3] interfacial polymerization,[10] and non-solvent-induced phase separation.[11] Most of those methods require the use of colloidal particles, surfactants, or block copolymers as templates in conjunction with sol-gel techniques. Once the organic templates are removed, pores form through thermal decomposition or solvent extraction. Such conventional methods usually require sacrificial templates, multiple-step preparation processes (e.g., direct templating methodology involves casting and template-removing processes), and specific materials.[1–3] Although alternative methods, such as non-solvent-induced phase separation, can also be used to simply prepare porous membranes or monoliths, such methods usually only work for a limited range of polymers.[11] From a practical point of view, a method that can generate micro/nanoscale porous structures in a wide range of polymer materials via a simple one-step process is highly desirable.

Recently, it has been demonstrated that the fabrication of a porous microstructure forms the basis of slippery surfaces.[12–14] The slippery phenomenon was first observed on the surface of the *Nepenthes* pitcher plant (**Figure 1**a).[12] When an insect attempts to land on the rim of a pitcher plant, it can hardly stand on it and, instead, will slide down from the rim to the bottom, which is filled with digestive juices. In addition to insects, a droplet of water or organic oil can freely slide

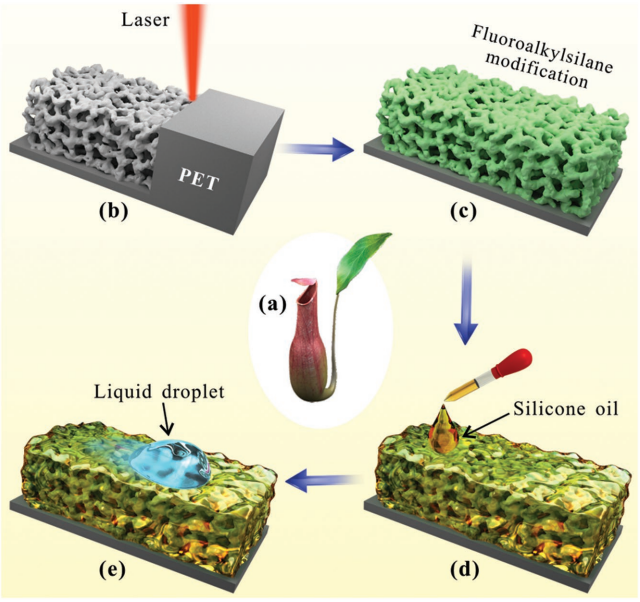

Figure 1. Schematic diagram of the preparation process for a slippery PET surface by femtosecond laser direct writing. a) Photo of the *Nepenthes* pitcher plant. b) Femtosecond laser ablation used to generate interconnected porous microstructures. c) Fluoroalkylsilane modification used to lower the surface free energy. Green color denotes the fluorosilane molecular layer. d) Infusion of the lubricating liquid (silicone oil) into the laser-induced micropores. e) Foreign liquid droplet sliding down the as-prepared slippery surface.

down the surface of a pitcher plant. There are many microscale pockets directionally distributed across the pitcher plant surface.[15,16] Every pocket consists of a micropore at the center. An intermediary liquid (called lubricating fluid) is locked into these micropores, resulting in a continuously trapped liquid cushion. Such a trapped lubricating layer can greatly decrease the pinning effect of the contact lines for various liquids, which endows the pitcher plant surface with excellent liquid-repellent property. Such a slippery surface is commonly called a "slippery liquid-infused porous surface (SLIPS)."[12] To design and fabricate such a liquid slippery surface, one needs to follow three criteria.[12,17] First, the substrate surface must have porous microstructures. These enable the lubricating liquid to wet and be firmly locked into the micropores. Second, the lubricating liquid should be more inclined to wet the solid substrate than the liquids that are to be repelled from it. Third, the lubricating liquid and the repelled liquids must be immiscible. If the micropores of the substrate surface are interconnected, the slippery surface may further show a self-repairing capability beyond the three requirements described above. For example, Wong et al. infused the lubricating liquid (fluoroalkylsilane) into the micropores of a structured Teflon surface, demonstrating an artificial SLIPS for the first time.[11] Liquid droplets were found to easily slide down the as-prepared SLIPS (tilted 5°). Most of the technologies reported to realize SLIPS are based on conventional bottom-up techniques, such as deposition and coating.[12–14] Porous networks are formed during the deposition/coating of nanoparticles or nanofibers onto a substrate. Generally, the porous layer and the substrate are different materials, so they have different mechanical, thermal, and electrical properties. Such a mismatch in properties can severely limit the range of application for as-synthesized SLIPS. A simple top-down method that can be used to directly build monolithic porous network microstructures (i.e., the porous layer and the substrate layer are inherently one and the same) for realizing a slippery property has been rarely reported.

Here, the fabrication of porous network microstructures based on a one-step femtosecond laser direct writing method on various polymer surfaces (including poly(ethylene terephthalate) (PET), poly(methyl methacrylate) (PMMA), polyamide (PA), polycarbonate (PC), polyethylene (PE), and polylactic acid (PLA)) was demonstrated. After laser ablation, the PET surface was fully covered with large numbers of protrusions and pores with diameters of several hundred nanometers. Then, the porous PET surface was further treated with fluoroalkylsilane, followed by the infusion of silicone oil. A slippery surface was obtained. Various liquid droplets were found to freely slide down the resulting surface, revealing excellent liquid repellency for the slippery surface. Furthermore, we found that the slippery surface and the original laser-induced porous PET surface played entirely different roles in the growth of C6 glioma cells.

By taking advantage of high precision processing, extensive materials processing, and strong controllability, femtosecond laser microfabrication has become an effective tool in the design and fabrication of complex 2D and 3D microstructures.[18–20] This technology can be used to directly form various micro/nanoscale hierarchical structures on a wide variety of materials surfaces through a one-step scanning process.[20–27] Figure 1b–e shows the process of fabricating a SLIPS based on femtosecond laser ablation. PET is a polymer that shows excellent optical and mechanical properties and a relatively high degree of biocompatibility.[28,29] PET is widely used in plastic products, with applications for film/sheet materials, bottle packaging, electronic appliances, auto parts, mechanical equipment, and so on. To generate a slippery porous layer covering the PET surface, a PET substrate was first ablated using a femtosecond laser via a typical line-by-line scan (Figure 1b). Then, the ablated sample was immersed into an alcohol solution of fluoroalkylsilane for 24 h to lower the surface free energy (Figure 1c). Finally, nonvolatile and eco-friendly silicone oil was selected as the lubricating fluid and dripped onto the fluorosilane-modified porous PET surface (Figure 1d). The silicone oil can fully wet and fill into the micropores due to the oleophilicity of the porous microstructures. At this point, a slippery property was realized, with various foreign liquid droplets observed to slide down the tilted slippery surface (Figure 1e).

A type of porous network microstructure can be directly formed on the PET surface by femtosecond laser ablation. **Figure 2**a–c shows the scanning electronic microscopy (SEM) images taken for a PET surface following femtosecond laser ablation at a laser power of 30 mW, scanning speed of 4 mm s^{-1}, and scanning-lines shift of 4 μm. The surface is textured to form a micro/nanoscale rough porous structure with large numbers of protrusions and pores (Figure 2a,b). The diameter of the protrusions is ≈1 μm, while that of the pores is only several hundred nanometers. A detailed SEM image reveals that

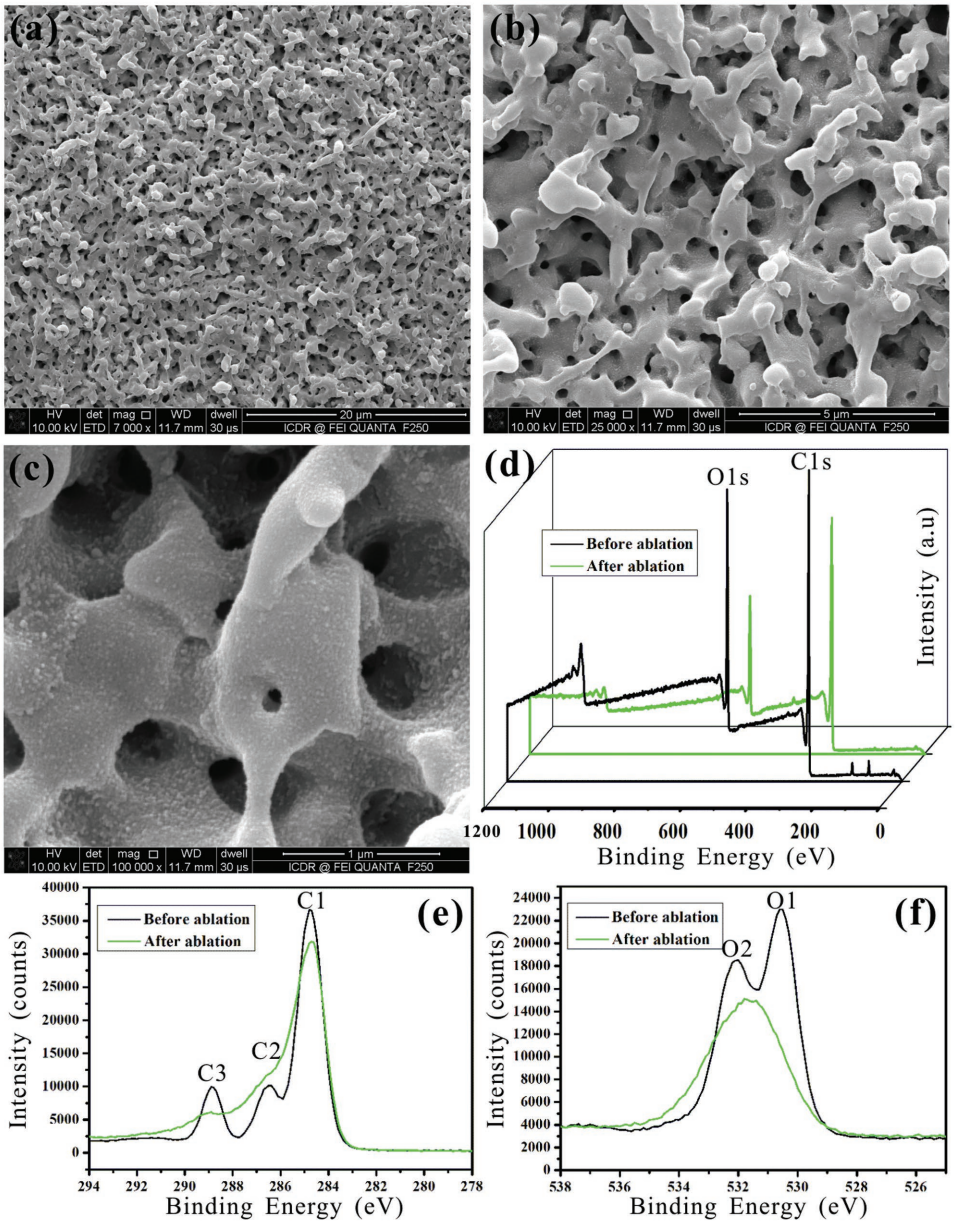

Figure 2. Microstructure and chemical composition of the femtosecond laser structured PET substrate. a–c) SEM images of the femtosecond laser ablated PET surface. XPS spectra of the untreated and laser-ablated PET surfaces: d) survey spectra, e) high-resolution spectrum for C 1s, and f) high-resolution spectrum for O 1s.

there is an abundance of nanoparticles with a size of 10–30 nm covering the surfaces of the microprotrusions and the walls of the micropores (Figure 2c). Such micropores can trap and host secondary liquid phases such as the lubricating liquid. In addition, the micropores connect with each other (rather than being independent of each other), resulting in a porous network microstructure. After femtosecond laser ablation, the transparent PET sheet showed a color change to an opaque color because of greater light scattering and refraction from the rough porous microstructures (Figure S1a, Supporting Information). The transmittance of the bare original PET surface decreased from ≈90% to <4% for the ablated surface in the visible wavelength region (Figure S1b, Supporting Information). The micropores become bigger, and their density decreases with an increase in scanning speed and scanning-lines shift to 6 mm s^{-1} and 6 µm, respectively (Figure S2a–c, Supporting Information). The porous network microstructure nearly disappears if the scanning speed and the scanning-lines shift are further increased to 8 mm s^{-1} and 8 µm, respectively (Figure S2d–f, Supporting Information). Since the PET substrate ablated at a laser scanning speed of 4 mm s^{-1} and shift of 4 µm shows the most rich porous network microstructures compared to other substrates, it is considered optimal for constructing a slippery surface.[12]

The formation of such a porous network microstructure is attributed to the interaction between the femtosecond laser and the PET surface. Laser ablation is one of the most commonly used techniques for direct writing various microstructures and generating micropatterns on the surface of semiconductors, metals, glasses, and polymers.[18,20,30] Since PET is a transparent and low light-absorbing polymer, it is not straightforward to ablate the PET surface using most conventional lasers because the photon energy is generally less than the bandgap of the polymer. Surprisingly, the energy transfer from a femtosecond laser pulse to a polymer surface can occur via a nonlinear absorption mechanism.[31,32] The photophysics of femtosecond laser ablation of polymers have been studied over the past two decades.[33–36] Avalanche ionization (AI) is the dominant absorption process for 50 fs pulses. Carriers that are thermally excited from traps or defects can usually act as the necessary seed electrons. Assuming that a small amount of seed electrons exists in the conduction band, AI can result in an exponential growth of conduction band electrons. On the other hand, high-intensity femtosecond laser pulses can also directly trigger AI by multiphoton ionization (MPI). Both AI and MPI are strongly laser intensity-dependent. When the laser pulse duration approaches the magnitude of a femtosecond, the instantaneous peak power is high enough to ionize almost any material surface.[33] The process of MPI and AI increases the density of free carriers in the plasma; meanwhile, the generated plasma continually absorbs the laser pulses until the plasma and the femtosecond laser have equal frequency. Following ionization, free electrons absorb the energy of the incident laser, rapidly increasing the kinetic energy of every free electron. A fraction of this energy is instantly transferred from the electrons to the lattice, leading to the formation of high-pressure and high-temperature (excess of 50 000 K) plasmas above the surface. Meanwhile, the electrons and ions reach thermal equilibration over a timescale of picoseconds. The ions instantaneously vaporize from the melt phase. Then, the plasma expands and bursts out of the focal volume because significant kinetic energy accumulates in the target material within the focal volume. Once the laser energy is high enough, micro/nanoscale hierarchical rough microstructures are usually generated by laser ablation. During the process of femtosecond laser ablation for the polymer materials, swelling, melting, and the formation of gaseous products (e.g., CO_2, CO) also occur.[37,38] The gas generated tends to pass through the molten region and eject from the bulk to the outside surface of the polymer. With the point of laser irradiation moving forward, the molten polymer present within the preceding focal volume instantaneously cools down and solidifies. As a result, the path travelled for the ejected gas is preserved in the form of interconnected microholes. On the other hand, material near the laser focus point can be removed and sputtered above the substrate during laser ablation. Such ejected material exists in the form of microscale or nanoscale molten particles. As the ejected particles fall back toward the substrate surface and recrystallize, the sample surface is finally covered with a layer of nanoparticles.[30]

The chemical change for the PET surface was analyzed by using an X-ray photoelectron spectrometer (XPS). Figure 2d shows the survey spectra of the PET samples measured before and after femtosecond laser ablation. The spectra for the two samples show two main peaks of carbon and oxygen. High-resolution spectra of the carbon C 1s peak for the untreated and laser ablated PET surfaces are shown in Figure 2e. The C 1s peak for the intrinsic PET is composed of three main components as follows: C1 at a binding energy of 284.8 eV that corresponds to C—C and C—H bonds (carbon atoms in phenyl ring); C2 at 286.4 eV that is attributed to C—O bonds (methylene carbon atoms singly bonded to oxygen); and C3 at 288.9 eV that is due to the O=C—O bond (ester carbon atoms).[39,40] Laser ablation leads to a decrease in intensity for both C1 and C3 peaks. The O 1s signal from the initial PET film showed two main peaks as follows: the O1 component at a binding energy of 530.5 eV due to the carbonyl O atoms (O=C) and the O2 component at 532 eV corresponding to ester O atoms (O—C) (Figure 2f). In addition, the O 1s signal shows a remarkable decrease following laser treatment. The O1 peak is observed to decrease more rapidly than the O2 peak after laser ablation. The decrease observed for C3 and O1 can be attributed to PET surface reorganization.[41–44] For example, decarbonylation and hydrogen abstraction might occur during femtosecond laser ablation of the PET substrate.[40,41] Moreover, small molecules such as CO_2 and CO are extracted from the PET surface, leading to the formation of terminate free radicals.[43,44] The photon absorption in PET can trigger two types of bond breaking: Norrish type I and II.[41,45] In Norrish type I, the C—H bonds at aromatic and aliphatic parts are decomposed. For Norrish type II, the C—C and C—O bonds in the main molecular chain are broken. Due to the ultrahigh instantaneous energy intensity of femtosecond laser pulses and the multiphoton-absorption process, both Norrish type I and II bond breaking can take place following irradiation of the PET substrate by femtosecond laser pulses. Based on the XPS results and the Norrish bond breaking principles, a possible mechanism is put forward for the reaction between the femtosecond laser and PET, as shown in **Scheme 1**.[41,42,45]

All of the flat, rough, and even fluorosilane-modified rough PET surfaces do not show liquid-repellent ability. A flat PET surface shows intrinsic hydrophilicity with a contact angle (CA) of 75.5 ± 3.5° for a water droplet (**Figure 3**a). The advancing CA (θ_{adv}) and receding CA (θ_{rec}) of a water droplet on such a surface is 79.9 ± 2.6° and 42.7 ± 3.7°, respectively; therefore, the CA hysteresis (θ_h), which is defined as the difference between θ_{adv} and θ_{rec}, is calculated to be 37.2° (**Table 1**). After the formation of a porous network microstructure by femtosecond laser ablation, the CA decreases to 29 ± 2° (Figure 3b). Such a significant decline in CA value indicates that the hydrophilicity of the PET surface is amplified by the laser-induced porous microstructures because the rough microstructures render the hydrophilic materials more hydrophilic.[17,46–48] In addition, the laser-induced surface polarity can also lead to increased hydrophilicity of the laser-treated PET. Fluorosilane modification is the most commonly used method for lowering the surface free energy of a solid substrate. When the porous PET surface was further modified with a fluoroalkyl layer (defined as F+Rough PET), water wettability switched from hydrophilicity to hydrophobicity. The CA of a water droplet on such a surface reaches up to 139 ± 1° (Figure 3c). Although the CA value is greatly increased and the contact area between the water droplet and

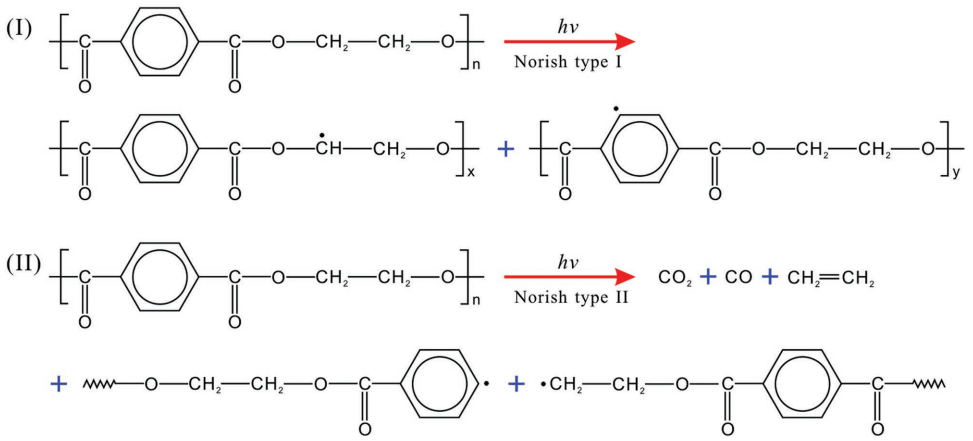

Scheme 1. Mechanism for femtosecond laser induced chemical change of the PET surface.

the substrate is reduced, the water droplet was observed to still firmly stick onto the PET surface, even when the substrate is positioned vertically or turned upside down (Figure 3d). The measured θ_h is as large as 134° (θ_{adv} = 152.8 ± 3.8° and θ_{rec} = 18.0 ± 1.8°), as shown in Table 1. In terms of oil wettability, the flat PET surface is intrinsically superoleophilic, with a CA of 6.7 ± 1.3° for an oil (hexadecane) droplet (Figure 3e). An oil droplet can fully spread out on the rough porous surface, resulting in a CA of ≈0° (Figure 3f). Although the surface becomes weakly oleophobic with the CA increasing to 103 ± 2.5° for an oil droplet on a fluorosilane-modified rough PET surface (Figure 3g), it is also found to firmly adhere to the substrate (Figure 3h). The θ_{adv}, θ_{rec}, and θ_h are 113.3 ± 2.1°, 9.6 ± 4.3°, and 103.7° against the hexadecane droplet. Therefore, all of the flat, rough, and fluorosilane-modified rough PET surfaces exhibit very large adhesion to both water droplets and organic oil droplets. Such surfaces are easily wetted or even contaminated by water and oils.

The SLIPS was fabricated by infusing silicone oil into the micropores of the fluorosilane-modified rough PET surface. In contrast to the flat, rough, and fluorosilane-modified rough PET surfaces, the silicone oil modified surface resulted in a slippery surface with strong water and oil repellence. Water (7 µL) and oil (7 µL) droplets can easily slide down such a slippery surface with tilt angle of 10°, as shown in Figure 3i,j and Movie S1 (Supporting Information). The average sliding speeds are 0.29 and 1.14 mm s^{-1} for a droplet of water and hexadecane, respectively. When the tilt angle of the substrate is lowered to 4°, the water and oil droplets can still slide downward, albeit more slowly (Movie S1, Supporting Information). The resultant SLIPS shows a very small θ_h of 0.6° against a water droplet (Table 1) and 0.2° against a hexadecane droplet. The silicone oil infused into the femtosecond laser patterned porous network can act as a lubricating layer, enabling water and oil droplets to freely slide down the slippery surface. Moreover, the as-prepared slippery surface can repel various other chemically pure or complex liquids, such as drinking water, milk, Coca-Cola, ink, coffee, fruit juice, glycerol, and egg white. These common, everyday liquids can easily slide down an ≈10° tilted slippery PET surface without staining, as shown in Figure 3k and Movie S2 (Supporting Information).

In addition to excellent liquid repellence, the as-prepared slippery surface shows high resistance to bending and friction. As shown in Figure S3a (Supporting Information), despite bending the slippery PET sheet until its two edges rolled up and contacted each other 50 times, the sliding angle of a droplet of water on such a surface was no more than 3°, indicating that the surface maintained its slippery property after being bent. To test the abrasion, the slippery PET sheet was pressed onto sandpaper (1000 mesh) and loaded with a 100 g weight. The sheet was then pulled forward a distance of 10 cm. The resulting abrasion for the slippery PET surface resulted in a slight increase of the water sliding angle to ≈5°, mainly because some lubricating liquid seeped into the sandpaper (Figure S3b, Supporting Information). However, by simply re-infusing the slippery PET sheet with lubricating liquid after being rubbed for different times, the water sliding angle for the surface was decreased to as low as 1.75–2.5°. The strong bend/abrasion-resistant ability of the femtosecond laser patterned slippery PET surface can be accounted for by the following: (1) the porous layer and the substrate are fabricated from the same material and are essentially monolithic, (2) PET is a stable material, and (3) the lubricating liquid trapped in the micropores affords a protective function for the porous network microstructure. Such stability is very important for widespread application of the slippery PET surface.

The femtosecond laser ablation can also be used to generate porous network microstructures in a wide range of other polymer materials, such as PMMA, PA, PC, PE, and PLA. **Figure 4** shows the SEM images of such polymers after femtosecond laser ablation. All of them were ablated using the same parameters as for PET (laser power = 30 mW, scanning speed = 4 mm s^{-1}, shift of the scanning lines = 4 µm). If the micropores of the surfaces are further infused with lubricating liquid, it is likely that all of these polymer substrates can become slippery surfaces.

The cell behavior at cell/material interfaces is closely related with the chemical and physical properties of the culture substrate, such as chemical composition, surface morphology, wettability, charge, and combinations of these properties.[49–54] Cell growth on flat and femtosecond laser structured porous polymer surfaces (including laser-induced rough surfaces and

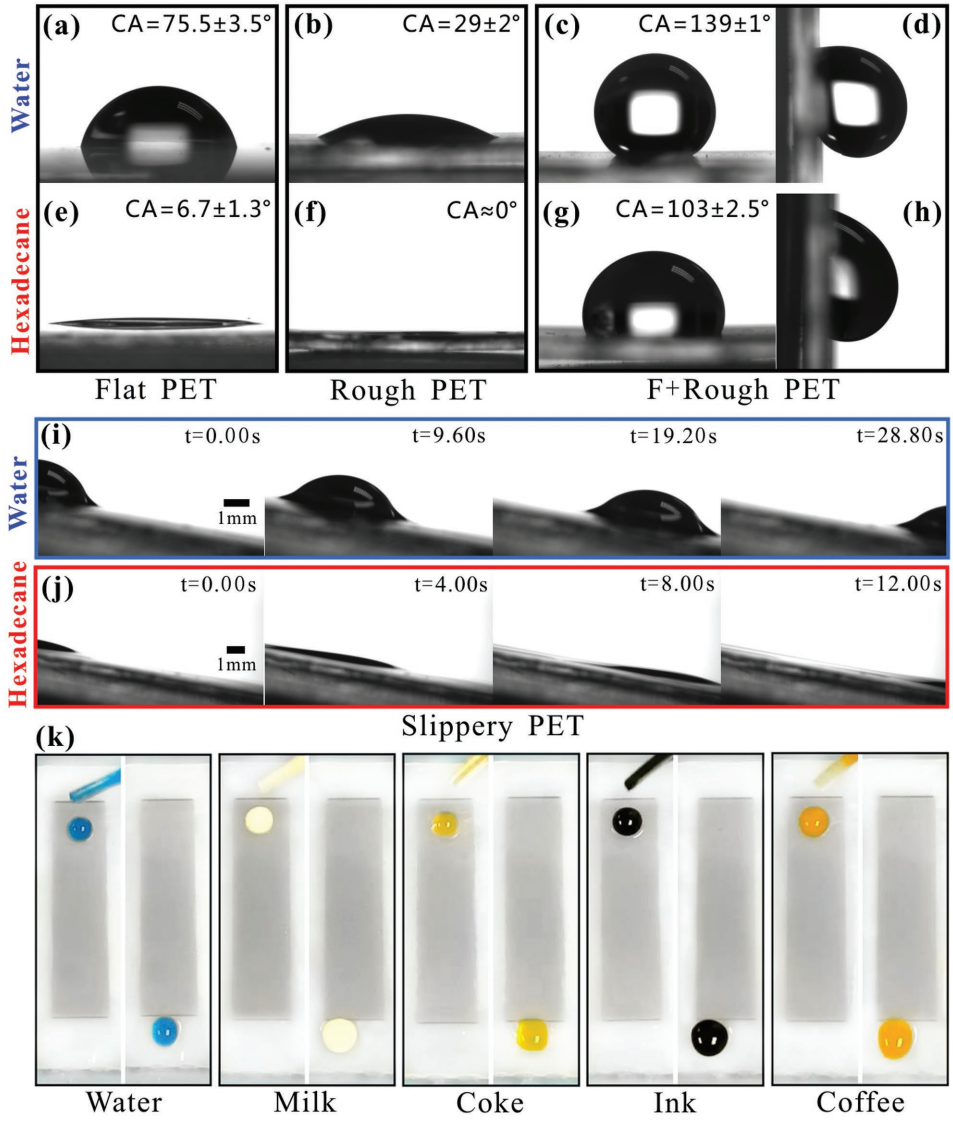

Figure 3. Different wettabilities of the flat, rough, fluorosilane-modified rough, and as-prepared slippery PET surfaces. a–d) Water droplet and e–h) hexadecane droplet a,e) on a flat PET surface, b,f) on a rough PET surface, c,g) on a fluorosilane-modified rough PET surface, and d,h) sticking onto a fluorosilane-modified rough PET surface. i) Water droplet and j) hexadecane droplet sliding down the as-synthesized slippery surface with tilt angle of 10°. k) Images of various liquids before and after sliding down the as-prepared slippery PET surface. The drinking water is dyed with methylene blue for improved observation.

slippery PET surfaces) were investigated using the C6 glioma cell as a test model because of wide study of its cytoskeleton arrangements and focal adhesion distribution on a textured substrate.[55] The C6 glioma cells were seeded on flat, rough, and slippery surfaces for 48 h. **Figure 5** shows the fluorescence microscopy images of the cell nucleus (blue) and cytoskeleton (red). Here, cell meshes are defined as the density of internal holes separated by staggered cell clusters in the cytoskeleton fluorescence microscopy image.[56] Figure 5a,d shows the original level for the number of C6 cells adhering to the intrinsic, hydrophilic smooth PET surface. The cells are normal in number with a density of ≈1349 mm^{-2} (**Figure 6**), and the meshes are virtually sparse. Compared to the flat surface, many more cells (≈3469 mm^{-2}) adhere to the laser-induced porous rough PET surface, with the mesh density significantly increased, indicating that the rough surface promotes cellular adhesion and proliferation of the C6 glioma cell (Figures 5b,e and 6). The cell

Table 1. Advancing contact angle (θ_{adv}), receding contact angle (θ_{rec}), and contact angle hysteresis (θ_h) of a water droplet on different PET substrates.

Surface type	θ_{adv}	θ_{rec}	θ_h
Flat PET	79.9 ± 2.6°	42.7 ± 3.7°	37.2
Rough PET	32.0 ± 5.4°	8.9 ± 2.5°	23
F+Rough PET	152.8 ± 3.8°	18.0 ± 1.8°	134
SLIPS	27.8 ± 0.1°	27.2 ± 0.1°	0.6

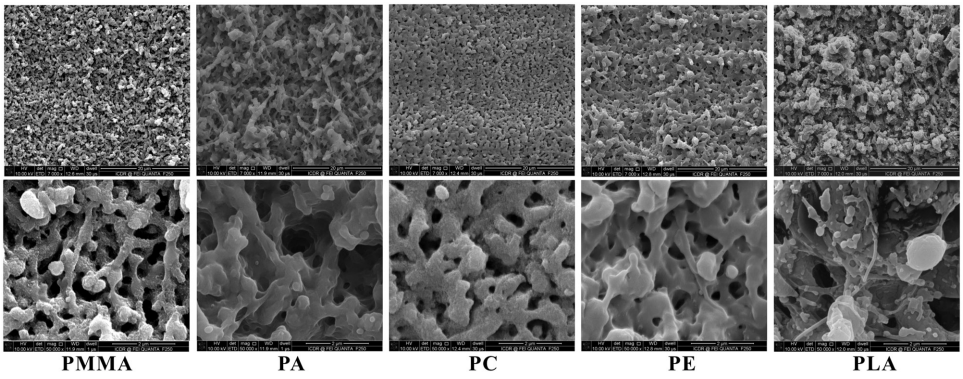

Figure 4. SEM images of various polymers surfaces after femtosecond laser ablation.

density on the rough porous surface is nearly 2.6 times that on the flat surface. Such enhanced proliferation is probably due to the combined action of the hydrophilicity and the hierarchical porous network microstructure of the ablated PET surface. In contrast, nearly no detectable adhered cells could be observed for the slippery surface in fluorescence images of both the cell nucleus and cytoskeleton (Figures 5c, f and 6). We conjecture that the anti-cell adhesion capability is probably due to the perfectly smooth surface formed following silicone oil treatment, which prevents topographic interaction between cells and the culture substrate.[57] The promotion and inhibition effect of the porous and slippery surface, respectively, on the activation and adhesion of C6 cells was further verified by observing the cell behavior at the boundaries between the flat area and the laser-induced rough area (Figure 5g), fluoroalkylsilane-modified flat area, and resultant slippery surface (Figure 5h,i). The effect of promoting cell growth for the laser-induced rough surface may be utilized for the preparation of cancer cell detectors, while the anti-C6-cell function of the slippery surface may be possibly applied as an implantable biological scaffold.

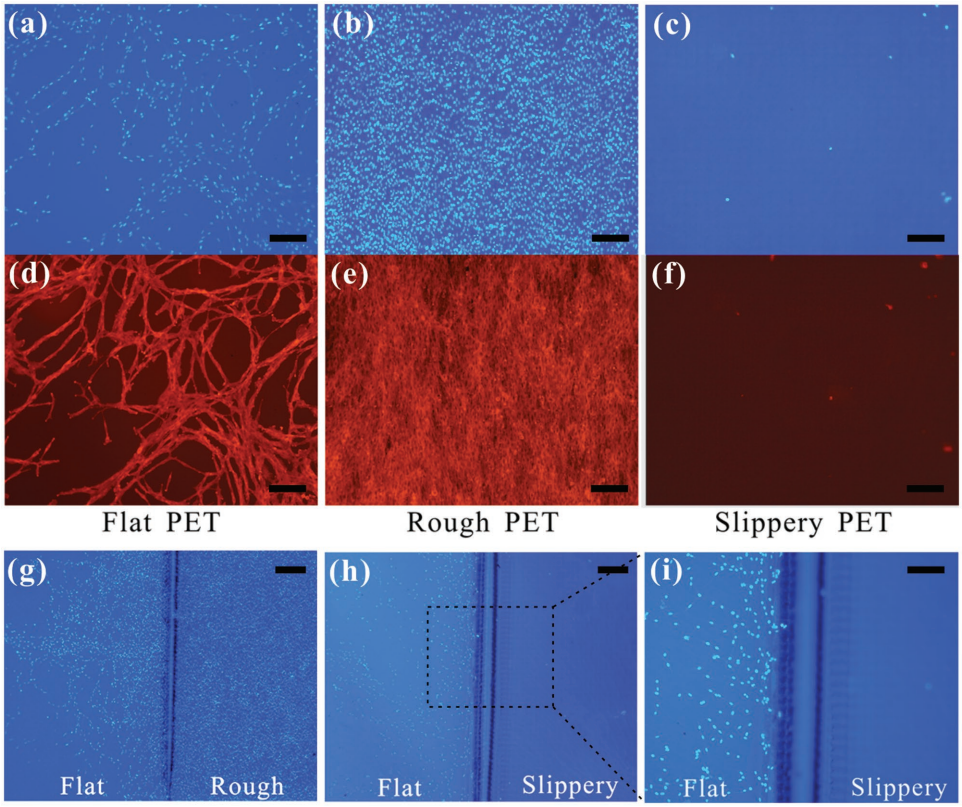

Figure 5. Cell growth of a C6 glioma cell on flat, rough, and slippery PET surfaces. The fluorescence microscopy images of a–c) cell nucleus (blue) and d–f) cytoskeleton (red) showing the cell quantity and actin cytoskeletal network on the a,d) flat PET, b,e) rough PET, and c,f) slippery PET surfaces. Comparison diagram for cell behavior at the boundaries between g) flat area and laser-induced rough area, h,i) fluoroalkylsilane-modified flat area, and resultant slippery surface. Scale bars: (a–f,i) 100 µm, (g,h) 200 µm.

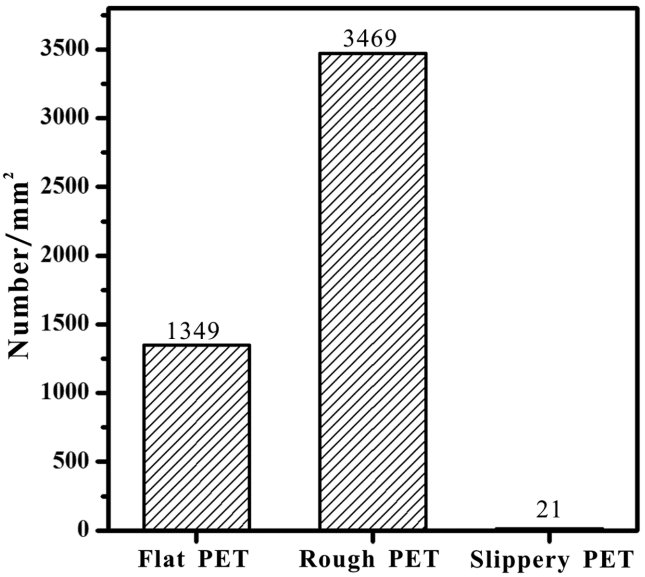

Figure 6. Statistical density of the C6 glioma cells on different PET surfaces.

A polymer-based porous network microstructure was simply formed on a PET surface by a one-step femtosecond laser direct writing method. Laser ablation resulted in the formation of an abundance of protrusions and pores, with a diameter of several hundred nanometers, completely covering the PET surface. Chemical treatment of the porous surface for further lowering of the surface free energy followed by the infusion of a lubricating liquid led to the preparation of SLIPS. The as-synthesized slippery surface showed excellent liquid-repellent ability. Various chemically pure or complex liquids (such as water, hexadecane, milk, Coca-Cola, ink, coffee, fruit juice, glycerol, and egg white) could freely slide down an ≈10° tilted slippery surface without leaving behind any stain. Compared to previously reported slippery surfaces, the porous layer and the substrate layer of the femtosecond laser-induced slippery surface are inherently one material. Furthermore, we found that the use of the original laser-induced porous PET surface as a culture substrate led to the promotion of the growth of C6 glioma cells, whereas the slippery PET surface completely inhibited C6 glioma cell growth. In addition, femtosecond laser ablation can be used to directly fabricate porous network microstructures for not just PET but an extremely wide range of polymers (PMMA, PA, PC, PE, PLA, etc.). Therefore, the femtosecond laser direct writing method can be used to enable almost all polymers to become a substrate of choice for constructing slippery surfaces. The cell-promoting/inhibiting ability of the femtosecond laser structured porous polymers shows potential for application in the patterning of cells and control of tissue formation.

Experimental Section

Femtosecond Laser Ablation: A PET sheet with a thickness of 0.3 mm was mounted onto a moveable platform. A Ti:sapphire femtosecond laser (Libra-usp-he, Coherent, USA) was utilized for generating microporous structures. The laser emitted 800 nm-center-wavelength pulses with a duration of 50 fs and repetition rate of 1 kHz. The laser beam was focused onto the PET surface by an objective lens (×20, NA = 0.40, Nikon, Japan) and used to irradiate the sample surface via line-by-line scanning. The laser power, scanning speed, and shift of the scanning lines were set at 30 mW, 4 mm s^{-1}, and 4 μm, respectively. The surface microstructures of samples ablated using different parameters were also investigated.

Infusion of Lubricating Liquid: After femtosecond laser ablation, a porous network microstructure was formed on the PET substrate. Then, the surface free energy of the porous sample was lowered by dipping the sample into a 0.5% fluoroalkylsilane (1H,1H,2H, 2H-perfluorodecyltrimethoxysilane) solution (in alcohol) for 12 h. The final step involved the infusion of lubricating fluid. In this experiment, silicone oil was selected as the lubricating liquid due to its eco-friendly and nonvolatile properties. Excess silicone oil was dripped onto the porous surface. The silicone oil was found to wet and infuse into the laser-induced micropores due to oleophilicity, resulting in the formation of a lubricating layer on the sample surface. Subsequently, excess oil was removed by holding the sheet vertically for a few minutes.

Cell Culture and Dye: The C6 glioma cells were seeded onto the prepared surfaces and cultured in high glucose DMEM supplemented with 10% fetal bovine serum (FBS, HyClone, GE Healthcare, USA), 100 U mL^{-1} penicillin (Beyotime, China), and 100 μg mL^{-1} streptomycin (Beyotime) at 37 °C in an atmosphere comprising 5% CO_2 and saturated humidity for 48 h. The cells were fixed with 4% paraformaldehyde for 10 min, washed three times with PBS and then permeabilized by 0.1% Triton X-100 for 3 min. 100×10^{-9} M of rhodamine phalloidin and 100×10^{-9} M of DAPI were used to stain the F-actin and cell nucleus, which were visualized by fluorescence microscopy.

Characterization: The surface topography of the polymers following femtosecond laser ablation was observed through a Quantan 250 FEG scanning electron microscope (FEI, America). The wettabilities for a deionized water droplet (≈7 μL) and hexadecane droplet (≈7 μL) on different types of PET surfaces were investigated by a JC2000D contact-angle system (Powereach, China). The chemical composition of the PET surface was characterized by XPS (AXIS ULtrabid, Kratos, England) using mono Al Kα operated at 150 W. The slippery properties of other various liquids (milk, Coca-Cola, ink, coffee, fruit juice, glycerol, and egg white) on the as-prepared substrate were also investigated.

Supporting Information

Supporting Information is available from the Wiley Online Library or from the author.

Acknowledgements

J.Y. and J.H. contributed equally to this work. This work was supported by the National Key Research and Development Program of China under Grant No. 2017YFB1104700, the National Science Foundation of China under Grant Nos. 51335008, 61475124, and 81371288, NSAF Grant No. U1630111, China Postdoctoral Science Foundation under Grant No. 2016M600786, the Collaborative Innovation Center of Suzhou Nano Science and Technology, and the International Joint Research Center for Micro/Nano Manufacturing and Measurement Technologies. The SEM work was done at the International Center for Dielectric Research (ICDR), Xi'an Jiaotong University.

Conflict of Interest

The authors declare no conflict of interest.

Keywords

femtosecond laser, inhibiting cell growth, porous polymers, SLIPS, superslippery surface

Received: November 14, 2017
Revised: December 28, 2017
Published online:

[1] D. Wu, F. Xu, B. Sun, R. Wu, H. He, K. Matyjaszewski, *Chem. Rev.* **2012**, *112*, 3959.
[2] X.-Y. Yang, L.-H. Chen, Y. Li, J. C. Rooke, C. Sanchez, B.-L. Su, *Chem. Soc. Rev.* **2017**, *46*, 481.
[3] Q. Liu, Z. Tang, B. Ou, L. Liu, Z. Zhou, S. Shen, Y. Duan, *Mater. Chem. Phys.* **2014**, *144*, 213.
[4] A. Thomas, F. Goettmann, M. Antonietti, *Chem. Mater.* **2008**, *20*, 738.
[5] A.-H. Lu, F. Schüth, *Adv. Mater.* **2006**, *18*, 1793.
[6] D. A. Olson, L. Chen, M. A. Hillmyer, *Chem. Mater.* **2008**, *20*, 869.
[7] M. R. Buchmeister, *Angew. Chem., Int. Ed.* **2001**, *40*, 3795.
[8] N. B. McKeown, P. M. Budd, *Macromolecules* **2010**, *43*, 5163.
[9] M. S. Silverstein, *Polymer* **2014**, *55*, 304.
[10] X. Zeng, D. Wu, R. Fu, *J. Appl. Polym. Sci.* **2009**, *112*, 309.
[11] Y. Xin, T. Fujimoto, H. Uyama, *Polymer* **2012**, *53*, 2847.
[12] T.-S. Wong, S. H. Kang, S. K. Y. Tang, E. J. Smythe, B. D. Hatton, A. Grinthal, J. Aizenberg, *Nature* **2011**, *477*, 443.
[13] U. Manna, D. M. Lynn, *Adv. Mater.* **2015**, *27*, 3007.
[14] S. Nishioka, M. Tenjimbayashi, K. Manabe, T. Matsubayashi, K. Suwabe, K. Tsukada, S. Shiratori, *RSC Adv.* **2016**, *6*, 47579.
[15] H. F. Bohn, W. Federle, *Proc. Natl. Acad. Sci. USA* **2004**, *101*, 14138.
[16] H. Chen, P. Zhang, L. Zhang, H. Liu, Y. Jiang, D. Zhang, Z. Han, L. Jiang, *Nature* **2016**, *532*, 85.
[17] J. L. Yong, F. Chen, Q. Yang, J. Huo, X. Hou, *Chem. Soc. Rev.* **2017**, *46*, 4168.
[18] K. Sugioka, Y. Cheng, *Appl. Phys. Rev.* **2014**, *1*, 041303.
[19] D. Wu, Q.-D. Chen, L.-G. Niu, J.-N. Wang, J. Wang, R. Wang, H. Xia, H.-B. Sun, *Lab Chip* **2009**, *9*, 2391.
[20] J. L. Yong, F. Chen, Q. Yang, X. Hou, *Soft Matter* **2015**, *11*, 8897.
[21] J. L. Yong, F. Chen, Q. Yang, G. Du, C. Shan, H. Bian, U. Farooq, X. Hou, *J. Mater. Chem. A* **2015**, *3*, 9379.
[22] J. L. Yong, F. Chen, Q. Yang, U. Farooq, X. Hou, *J. Mater. Chem. A* **2015**, *3*, 10703.
[23] J. L. Yong, F. Chen, Q. Yang, Y. Fang, J. Huo, X. Hou, *Chem. Commun.* **2015**, *51*, 9813.
[24] J. L. Yong, F. Chen, Q. Yang, D. Zhang, U. Farooq, G. Du, X. Hou, *J. Mater. Chem. A* **2014**, *2*, 8790.
[25] J. L. Yong, F. Chen, Q. Yang, Y. Fang, J. Huo, J. Zhang, X. Hou, *Adv. Mater. Interfaces* **2017**, *4*, 1700552.
[26] J. L. Yong, Y. Fang, F. Chen, J. Huo, Q. Yang, H. Bian, G. Du, X. Hou, *Appl. Surf. Sci.* **2016**, *389*, 1148.
[27] J. L. Yong, F. Chen, Y. Fang, J. Huo, Q. Yang, J. Zhang, H. Bian, X. Hou, *ACS Appl. Mater. Interfaces* **2017**, *9*, 39863.
[28] J. M. Goddard, J. H. Hotchkiss, *Prog. Polym. Sci.* **2007**, *32*, 698.
[29] S. B. Amor, M. Jacquet, P. Fioux, M. Nardin, *Appl. Surf. Sci.* **2009**, *255*, 5052.
[30] A. Y. Vorobyev, C. Guo, *Laser Photonics Rev.* **2013**, *7*, 385.
[31] D. von der Linde, K. Sokolowshi-Tinten, J. Bialkowski, *Appl. Surf. Sci.* **1997**, *109*, 1.
[32] K. Sokolowshi-Tinten, J. Bialkowski, A. Cavalleri, D. von der Linde, *Phys. Rev. Lett.* **1998**, *81*, 224.
[33] D. B. Wolfe, J. B. Ashcom, J. C. Hwang, C. B. Schaffer, E. Mazur, G. M. Whitesides, *Adv. Mater.* **2003**, *15*, 62.
[34] K. S. Tiaw, S. W. Goh, M. Hong, Z. Wang, B. Lan, S. H. Teoh, *Biomaterials* **2005**, *26*, 763.
[35] S. Baudach, J. Bonse, J. Krüger, W. Kautek, *Appl. Surf. Sci.* **2000**, *154*, 555.
[36] S. Baudach, J. Bonse, W. Kautek, *Appl. Phys. A* **1999**, *69*, S395.
[37] T. Efthimiopoulos, C. Kiagias, G. Heliotis, E. Helidonis, *Can. J. Phys.* **2000**, *78*, 509.
[38] J. Krüger, S. Martin, H. Mädebach, L. Urech, T. Lippert, A. Wokanu, W. Kautek, *Appl. Surf. Sci.* **2005**, *247*, 406.
[39] M. Kormunda, J. Pavlik, *Polym. Degrad. Stab.* **2010**, *95*, 1783.
[40] A. Vesel, M. Mozetic, A. Zalar, *Vacuum* **2008**, *82*, 248.
[41] G. Wu, M. D. Paz, S. Chiussi, J. Serra, P. González, Y. J. Wang, B. Leon, *J. Mater. Sci.: Mater. Med.* **2009**, *20*, 597.
[42] M. Dadsetan, H. Mirzadeth, N. Sharifi, *Radiat. Phys. Chem.* **1999**, *56*, 597.
[43] M. Chtaib, E. M. Roberfroid, Y. Novis, J. J. Pireaux, R. Caudano, *J. Vac. Sci. Technol.* **1989**, *7*, 3233.
[44] S. Lazare, R. Srinivasan, *J. Phys. Chem.* **1986**, *90*, 2124.
[45] Y. G. Yingling, B. J. Garrison, *J. Phys. Chem. B* **2005**, *109*, 16482.
[46] Y. Tian, B. Su, L. Jiang, *Adv. Mater.* **2014**, *26*, 6872.
[47] L. Wen, Y. Tian, L. Jiang, *Angew. Chem., Int. Ed.* **2015**, *54*, 3387.
[48] J. L. Yong, F. Chen, M. Li, Q. Yang, Y. Fang, J. Huo, X. Hou, *J. Mater. Chem. A* **2017**, *5*, 25249.
[49] A. L. Hook, N. H. Voelcker, H. Thissen, *Acta Biomater.* **2009**, *5*, 2350.
[50] X. Liu, S. Wang, *Chem. Soc. Rev.* **2014**. *43*, 2385.
[51] C. Simitzi, A. Ranella, E. Stratakis, *Acta Biomater.* **2017**, *51*, 21.
[52] S. M. Oliveira, W. Song, N. M. Alves, J. F. Mano, *Soft Matter* **2011**, *7*, 8932.
[53] W. Cheng, L. Ding, S. Ding, Y. Yin, H. Ju, *Angew. Chem., Int. Ed.* **2009**, *48*, 6465.
[54] W. Feng, L. Li, E. Ueda, J. Li, S. H, A. Welle, O. Trapp, P. A. Levkin, *Adv. Mater. Interfaces* **2014**, *1*, 1400269.
[55] B. Zhu, Q. Zhang, Q. Lu, Y. Xu, J. Yin, J. Hu, Z. Wang, *Biomaterials* **2004**, *25*, 4215.
[56] C.-H. Lee, Y.-W. Cheng, G. S. Huang, *Nanoscale Res. Lett.* **2014**, *9*, 250.
[57] G. Li, G. Yang, P. Zhang, Y. Li, J. Meng, H. Liu, S. Wang, *Small* **2015**, *11*, 5642.